Large-Scale Metasurfaces Made by an Exposed Resist

Citation for the original published paper (version of record):
Andrén, D., Martinez Llinas, J., Tassin, P. et al (2020). Large-Scale Metasurfaces Made by an Exposed Resist. ACS Photonics, 7(4): 885-892. http://dx.doi.org/10.1021/acsphotonics.9b01809

ACS Photonics

pubs.acs.org/journal/apchd5

Letter

Large-Scale Metasurfaces Made by an Exposed Resist

Daniel Andrén,* Jade Martínez-Llinàs, Philippe Tassin, Mikael Käll,* and Ruggero Verre*

Cite This: *ACS Photonics* 2020, 7, 885−892

Read Online

ACCESS | Metrics & More | Article Recommendations | Supporting Information

ABSTRACT: Phase-gradient metasurfaces have the potential to revolutionize photonics by offering ultrathin alternatives to a wide range of common optical elements, including bulky refractive optics, waveplates, and axicons. However, the fabrication of state-of-the-art metasurfaces typically involves several expensive, time-consuming, and potentially hazardous processing steps. To address this limitation, a facile methodology to construct phase-gradient metasurfaces from an exposed standard electron beam resist is developed. The method dramatically cuts the required processing time and cost as well as reduces safety hazards. The advantages of the method are demonstrated by constructing high-performance flat optics based on the Pancharatnam-Berry phase gradient concept for the entire visible wavelength range. Manufactured devices include macroscopic (1 cm diameter) positive lenses, gratings exhibiting anomalous reflection, and cylindrical metalenses on flexible plastic substrates.

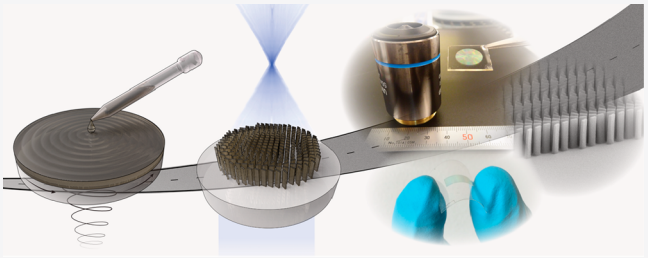

KEYWORDS: *flat optics, phase gradient metasurfaces, metalenses, nanofabrication, flexible optics*

Phase-gradient metasurfaces allow the phase profile of a transmitted or reflected light wave to be arbitrarily controlled by engineering the properties and spatial arrangement of the constituent subwavelength elements, the "meta-atoms".[1,2] This concept has enabled the realization of flat counterparts to most common optical elements, including lenses,[3−11] holograms,[12−14] beamsplitters,[15,16] curved mirrors,[17] and retroreflectors,[18] in some cases even outperforming their bulk counterparts by some figures of merit. As the field has matured, researchers have also turned to designing more exotic metasurfaces capable of performing tasks usually requiring an entire optical setup, such as optical tweezers,[19,20] planar cameras,[21] light-field imaging systems,[22] color routing,[23] spectrometers,[24] dynamic optical elements,[25−27] and super-resolution imaging components.[28,29]

Metasurfaces are thus improving at an impressive pace; however, contemporary systems still have shortcomings that need to be overcome for flat optical components to reach their full potential. Most importantly, state-of-the-art metasurfaces are currently fabricated by highly demanding procedures that typically involve deposition of a transparent dielectric, such as TiO_2,[6,9] GaN,[7] Si_3N_4,[11] or Si (in the NIR range),[8,15] followed by lithographic patterning, additional depositions, etching, and so on. A cost-effective alternative material platform and fabrication method that is accessible, scalable, and based on only nontoxic disposable materials could dramatically accelerate the impact of metasurface flat optics across society.

Here, we propose and demonstrate such a system based on the use of a standard negative resist that is hardened through electron beam exposure and that, if properly patterned, can form the metasurface itself (Figure 1). This effectively reduces the required fabrication to a single lithography step and removes any subsequent need for material deposition, lift-off, or etching. Polymers have been used as building blocks for traditional diffractive optics elements[30−32] but so far not explored in the context of phase gradient metasurfaces. By correct optimization, we realized a variety of polymer metasurfaces, including macroscopic flat optics and flexible elements, with efficiencies above 50% across the visible spectrum, in a fraction of the time needed when using established manufacturing methods. The methodology is readily adaptable to deep UV-lithography, thus, paving the way for mass production of flat consumer optics.

OPTIMIZATION OF NANOFIN DIMENSIONS

We choose an off-the-shelf negative electron beam lithography (EBL) resist (ma-N 2410, Micro Resist Technology GmbH), with comparatively high refractive index and low absorption, as our material system (Figure S1). The resist is spin-coated to the desired thickness on an arbitrary substrate and then patterned in a single EBL exposure, yielding high aspect ratio nanofins suitable as Pancharatnam-Berry (PB) metasurface building blocks. This approach utilizes that an individual nanofin can function as a subwavelength half-wave plate due to its shape birefringence. Thus, an incident circularly polarized wave can be

Received: December 22, 2019
Published: March 19, 2020

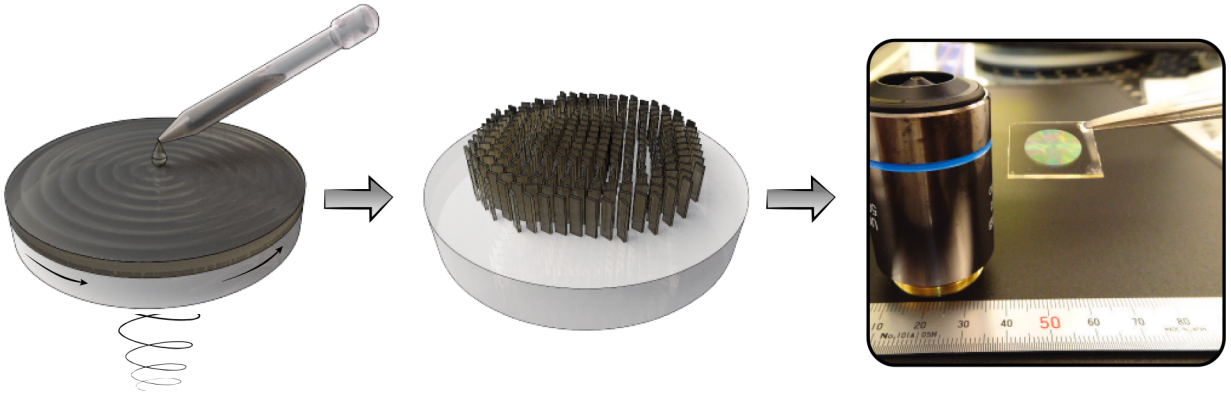

Figure 1. Metasurfaces can be made by an exposed negative electron beam resist as the sole constituent material. The method involves spin coating of a standard electron beam resist, prebaking, e-beam exposure, and development. This protocol eliminates any need for additional material deposition, lift-off, or etching. A macroscopic metasurface flat lens can be made from start to finish within a few hours, significantly faster than any existing EBL-based method.

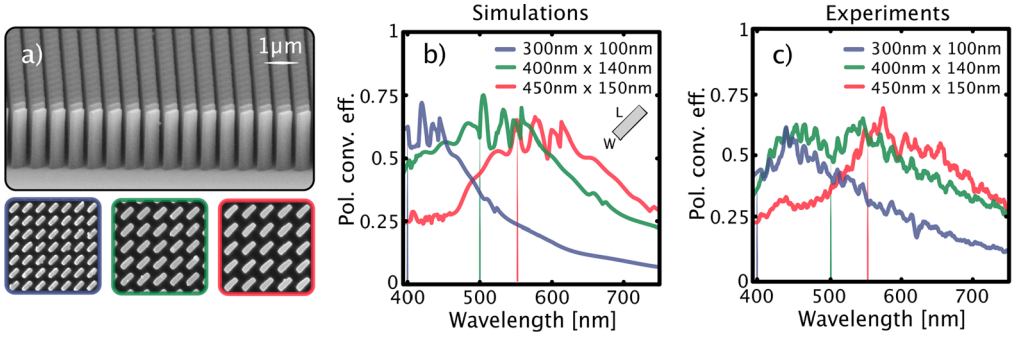

Figure 2. Birefringent nanofins made of the exposed resist can be used to realize efficient metasurfaces. (a) Tilted and top view SEM images of the resist metasurfaces. The frame colors of the lower images correspond to the metasurfaces measured in (c). (b) Simulated and (c) experimental polarization conversion efficiency spectra for metasurfaces optimized for blue, green, and red light. The nanofins are oriented at 45° from the axes of a square lattice with periodicity D, indicated by the vertical lines.

flipped to the opposite handedness. By varying the rotation angle θ_{rot} of each nanofin across a lattice, it is possible to impose a spatially varying phase profile $\varphi(\mathbf{r}) = 2\theta_{rot}(\mathbf{r})$ to the cross-polarized transmitted or reflected waves.[4,33−37] Given that the lattice constant is small compared to the selected operation wavelength and that the polarization conversion efficiency is high, this means that the metasurface in principle can be designed to impart any arbitrary phase profile simply by selecting the orientation of each subwavelength element. The PB phase concept has proven to be extremely powerful for designing a wide range of broadband phase-gradient metasurfaces and flat optical components.[6−8]

To obtain optimized design parameters for metasurfaces working in the visible wavelength range, we first performed finite difference time-domain (FDTD) simulations using in-plane periodic boundary conditions. We analyzed the polarization conversion efficiency for nanofins on glass in air as a function of in-plane dimensions (length L, width W), height H, and lattice constant D. Initial simulation results indicate that the polarization conversion efficiency scales almost linearly with nanofin height for given in-plane dimensions (Figure S2). Hence, care should be taken to maximize this value experimentally. Using standard process parameters, it is possible to obtain nanofins with an out-of-plane aspect ratio (H/W) of around 10. Unfortunately, for higher aspect ratios, water rinsing and subsequent nitrogen drying after development cause the nanofins to collapse due to surface tension forces (Figure S3). However, this well-known issue can be circumvented by using so-called critical point drying with surfactant-modified hexane as the intermediary liquid (see Methods for details).[38−40] This methodology allowed us to routinely fabricate nanofins with aspect ratios approaching 20 (Figure 2a).

The simulations allow us to optimize three nanofin dimensions for operation in the blue, green, and red wavelength ranges. The simulated efficiency spectra (Figure 2b) peak above 50% for specific wavelengths and dimensions are in excellent overall agreement with the experimental results (Figure 2c, see Figure S4 for experimental setup and details). Both experiments and theory indicate a broad range of operation around the chosen design wavelengths, although lattice modes, caused by diffractive coupling within the nanofin layer, induce rather sharp spectral fluctuations in efficiency. Nevertheless, the simulations show almost constant transmission efficiency versus nanofin orientation and homogeneous phase coverage (Figure S5) and the measured transmission coefficients at the respective design wavelengths are almost independent of metasurface orientation (Figure S6). Calculations of near-field intensity distributions along the two in-plane principal axes verify that the nanofins support waveguiding modes (Figure S7). Such modes are known to contribute to phase accumulation in PB metasurfaces[10] and they are fundamental also to polarization-independent uniform waveguiding metasurfaces.[41,42]

https://dx.doi.org/10.1021/acsphotonics.9b01809
ACS Photonics 2020, 7, 885−892

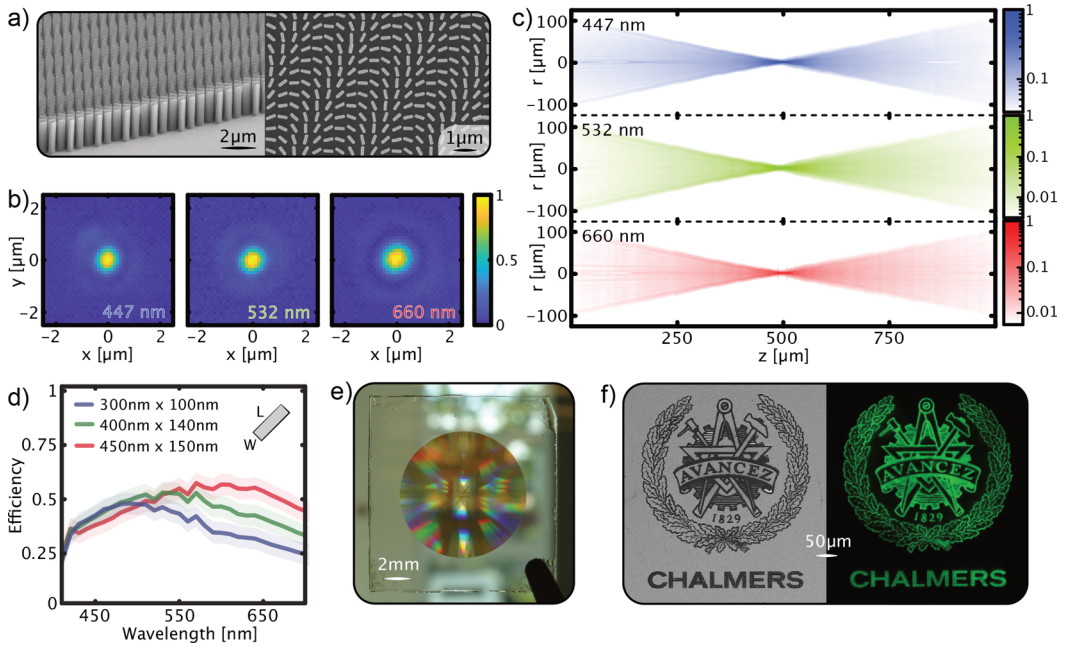

Figure 3. Transmissive resist metalenses for focusing and imaging. (a) Tilted and top view SEM images of metalens sections. (b) Focal spots produced by three lenses with $f = 100$ μm and NA = 0.65 designed for blue, green, and red light and measured using laser illumination with $\lambda_0 = 447$, 532, and 660 nm, respectively. Each lens exhibits a near diffraction-limited focus with Airy disk diameters of ∼500, 550, and 600 nm, respectively. (c) Measured intensity profiles along the optical axis of three lenses designed to have $f = 500$ μm and a NA = 0.24 for the same laser wavelengths as in (b). Note the normalized logarithmic intensity scale. (d) Measured polarization conversion efficiency spectra of the lenses in (c). The shaded regions represent an estimated ±5% error margin. (e) Picture of a 1 cm metalens with $f = 4$ mm. (f) SEM image (left) and optical image produced by the 1 cm metalens (right) of a transmissive test target etched out from an opaque Cr film. The Chalmers logo and Avancez mark are published with permission by the Chalmers University of Technology.

SPHERICAL METALENS

To demonstrate the application potential of the resist metasurfaces, we subsequently realized a variety of flat positive lenses, arguably the most used and important element in applied optics. The phase profile required to achieve lensing is $\varphi(r) = \frac{2\pi}{\lambda_0}(f - \sqrt{r^2 + f^2})$, where r is the radial distance from the optical axis, f is the focal length, and λ_0 is the free-space wavelength.[3] Based on the PB phase concept, we designed lenses of different focal lengths for blue, green, and red light using the same optimized nanofin and unit cell dimensions as in Figure 2. Figure 3a exemplifies the resulting structures. The focusing ability of the lenses were quantified using collimated circularly polarized laser light (λ_0 = 447, 532, and 660 nm; see Figure S8 for the optical setup). Figure 3b shows focal spot images for lenses designed with $f = 100$ μm and numerical aperture NA = 0.65. The central disks of the characteristic Airy patterns have full widths at half maxima (fwhm) of ∼500, 550, and 600 nm for the blue, green, and red laser wavelengths, respectively. The focal spots are thus broader than the diffraction limit ($\sim\lambda_0$/2NA), likely due to the sharp phase profile at the periphery of the lens not being properly reproduced by the chosen meta-atom unit-cell. Yet, the focusing properties are similar to what is typically seen for standard microscope objectives with similar f and NA. Furthermore, the intensity distribution along the optical axis shows characteristic Gaussian intensity profiles, as demonstrated in Figure 3c for lenses designed with $f = 500$ μm and NA = 0.24. We also verified that the polarization conversion efficiencies of the metalenses were comparable to the results obtained for the corresponding homogeneous nanofin arrays (Figure 3d). In this case, the laser light source was replaced by a white-light source together with a liquid crystal tunable filter, with which hyperspectral imaging and polarization optics were used to measure the efficiency spectra of the metalenses.

To demonstrate the potential for realizing macroscopic optical components using the resist methodology, we fabricated a 1 cm diameter flat lens designed for 532 nm light (Figure 3e). Although the lens consists of >600 million individual elements, the facile fabrication process allows the lens to be finalized in a single afternoon of lab work, including sample preparation, EBL exposure, and development.

Figure 3f illustrates the imaging performance of the macroscopic metalens. The test target, a 400 μm diameter version of our university logo etched out from an opaque chromium film (Figure 3f, left) was placed in the object plane of an imaging system in which the metalens acts as an infinity-corrected microscope objective (Figure S9). The test target was backlit by diffuse circularly polarized 532 nm light and the magnified image was projected onto a screen and photographed.[6] The resulting image clearly displays even the finest details of the target (Figure 3f, right; see also Figure S10 for images of a standardized resolution test chart, 1951 USAF).

SUBSTRATE-INDEPENDENT PROCESSING

The advantages offered by the resist methodology go beyond simplicity and scalability. In particular, the method can be adapted to practically any substrate and requires processing temperatures as low as 90 °C. This is a significant advantage compared to established techniques, which rely on high-temperature material growth (e.g., metallo-organic chemical vapor deposition) or the use of nonconventional chemicals (e.g., atomic layer deposition techniques). As examples of substrate independence, we fabricated metasurfaces on flexible plastic

https://dx.doi.org/10.1021/acsphotonics.9b01809
ACS Photonics 2020, 7, 885−892

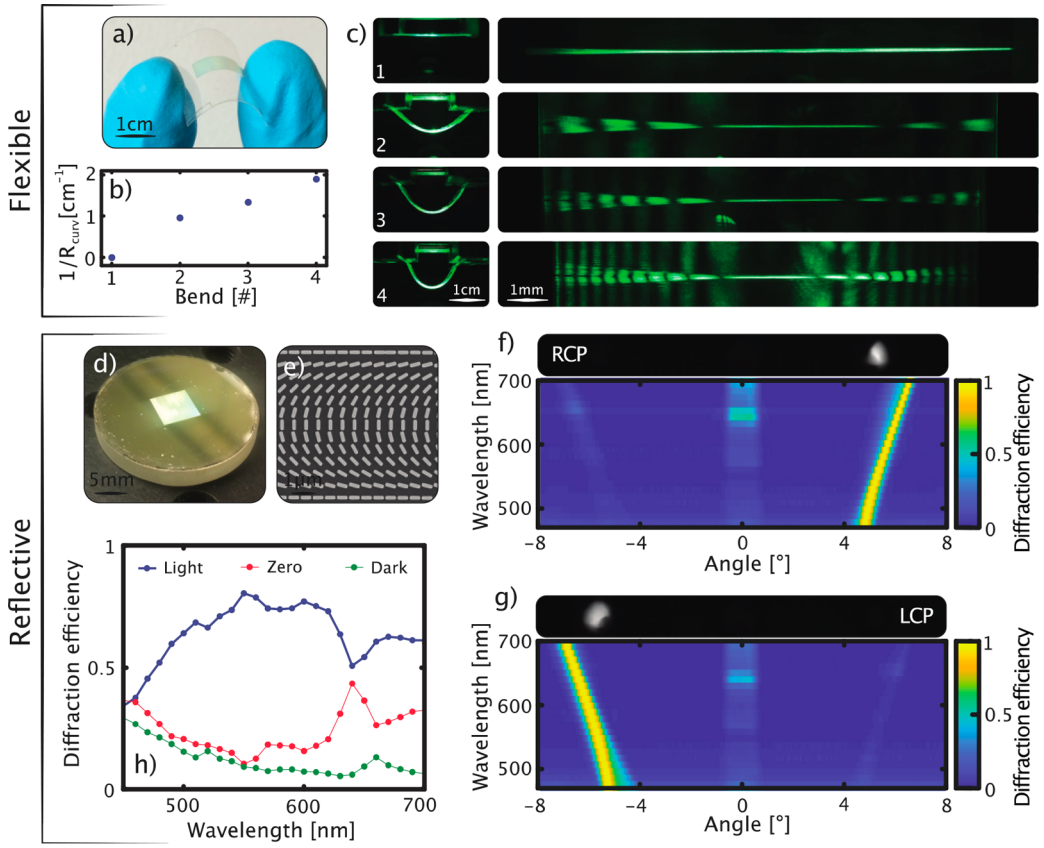

Figure 4. Resist metasurfaces on flexible and reflective substrates. (a) Picture of a flexible metasurface cylindrical lens during deformation. (b) Inverse radius of curvature for four degrees of bending where the *x*-axis numbers correspond to the ones in the left column of (c). (c) Left column displays top-view images of the flexible metasurface during operation. Right column presents how the in-plane line focus produced by the cylindrical lens is modified by varying the radius of curvature. The vertical lines are induced by stress-induced birefringence in the substrate. (d) Photograph of the reflective metasurface fabricated on a SiO_2-coated silver mirror. (e) Top-view SEM image of a section of the linear phase gradient metasurface, showing the superstructure-unit cell. (f, g) Normalized reflected intensity versus wavelength and diffraction angle for (f) right-handed and (g) left-handed circularly polarized light under normal incidence. The top insets show Fourier images recorded at the wavelength with highest polarization conversion efficiency ($\lambda \approx 550$ nm). (h) Relative intensity in the zeroth and ±first (bright and dark) reflected diffraction orders for normal incidence and circular polarization.

substrates (polyethylene terephthalate, PET) and on metal mirrors (Figure 4).

Figure 4a–c shows a 4×10 mm^2 cylindrical metasurface lens with $f = 1$ cm fabricated on a flexible PET substrate. Bending the substrate along the direction of the phase gradient (Figure 4a) results in a curved line focus with focal length curvature determined by the degree of bending (Figure 4b and left column of Figure 4c). Therefore, if the central part of the line is focused on a flat screen oriented orthogonal to the optical axis, the peripheral parts of the line will appear blurry since their corresponding focal points are located in front of the screen. This effect increases with the amount of bending (Figure 4c). The images of the curved line foci also display periodic bright and dark bands due to stress-induced birefringence in the PET substrate. These artifacts are likely to disappear with gentle thermal annealing of the substrate in the curved position. Additionally, we note that the function of the flexible metalens did not degrade noticeably even after repeated bending of the substrate to a radius of curvature smaller than half a centimeter.

The possibility to build reflective metaoptics using the resist methodology was demonstrated by fabrication of linear phase gradient metasurfaces[2,15] on commercially available coated silver mirrors (Figure 4d) and on optically thick gold films deposited in-house (Figure S11). The metasurfaces were constructed from the same optimized nanofin design as above, but the nanofins are now arranged in a super cell consisting of 12 nanofins successively rotated by 15° in one direction and repeated in the other one (Figure 4e). The result is a metasurface that acts as a polarization sensitive blazed grating able to distinguish the handedness of light via anomalous reflection.[2] Figure 4f-g show the spectral variation of the reflected intensity for incident right/left-handed circularly polarized light versus emission angle (see Figures S12 and S13a,b for experimental and spectral details). The effect of the phase profile can be seen from the relative intensities of the ±first-order diffraction lines, which are either strongly enhanced or suppressed at opposite sides of the specular zeroth order diffraction. This exotic behavior is easily observed by the naked eye in ambient lighting (Figure S13c–e). We quantified the diffraction efficiency by normalizing the intensities in the different diffraction orders to the total reflected intensity (Figure 4h). At the optimal working wavelength around 550 nm, the metamirror directs ~80% of the reflected light to either left or right depending on the handedness of the impinging circularly polarized wave. The overall reflectivity of the metamirror is ~50% (referenced to a plain silver mirror), but this value would likely increase with further optimization.

https://dx.doi.org/10.1021/acsphotonics.9b01809
ACS Photonics 2020, 7, 885–892

CONCLUSIONS

We have shown that it is possible to build optical metasurfaces with an off-the-shelf electron beam resist as the only constituent material. This makes it possible to avoid most of the time-consuming, costly and sometimes hazardous processing steps typically involved in building phase gradient metasurfaces. The resulting metasurfaces are efficient (polarization conversion >50%) and function across the entire visible wavelength spectrum. As a proof-of-principle, we developed the flat optical equivalent of spherical lenses, which show both narrow focusing and high-resolution imaging. Moreover, the method is compatible with a wide range of substrates, as demonstrated through the realization of metasurfaces on both flexible plastic supports and metallic mirrors. The possibility to construct metasurfaces on flexible or conformable substrates open new avenues for combining flexible electronics with flat optical devices[43,44] and could enable the realization of, for example, tunable attenuators by inducing specific deformations of the substrate. Furthermore, reflective hybrid metallic/dielectric metasurfaces have been proposed as a platform for new optical phenomena.[17,45] Although we have here focused on constructing geometrical (Pancharatnam-Berry) metasurfaces, the methodology can also be used to build polarization independent uniform waveguiding metasurfaces, since the resist metaatoms are found to support clear waveguiding modes.

The macroscopic metasurfaces (1 cm in diameter) are made possible by using high EBL writing speeds, partly by the use of a large beam current and partly by the relatively high sensitivity of the ma-N 2410 resist, which can be exposed with low doses. However, we note that even shorter writing speed could be achieved with other resists that are up to 100 times more sensitive (such as the UV−N series). During the design stage, files of sizes larger than 50 GB needed to be handled, potentially posing some memory limitations if even larger metasurfaces should be realized. However, such restrictions could be surmounted by clever design and processing algorithms designed for large-scale metasurfaces.[46,47]

The metasurfaces are stable over time and can be left in ambient conditions without any noticeable degradation for at least six months. Regarding stability, the polymer metasurfaces withstand temperatures at least as high as 100 °C and relatively high light intensities (up to 5 W/cm^2 generated by a 532 nm continuous laser source), without any apparent reduction in the metasurface performance. It might be possible to apply a thin (<10 nm) conformal protective coating (e.g., via atomic layer deposition) to the metasurfaces to improve their thermal stability and slightly increase the refractive index contrast to the surrounding. Moreover, for practical use, it will be necessary to protect the delicate nanostructures from abrasion. The simplest way of doing that would be to simply place a cover glass in front of the surface, as routinely done for protecting sensitive image sensors in current commercial products.

One weakness with metasurfaces in general is the inherent chromatic aberrations induced by the material dispersion as well as the design of the phase profile. This issue is of minor importance in narrow-band applications, in particular involving lasers, which is thus where flat optical elements are likely to first become truly competitive. Yet, there are plenty of ongoing efforts toward realizing achromatic flat optical components.[7,14,29,48,49] Since the refractive index dispersion of polymers are generally quite low, the technique presented in this article might prove useful in such endeavors.

The fabrication technique presented here is accessible also to laboratories and researchers that lack access to the advanced tools for material growth, deposition, and etching, typically required for metasurface fabrication. Although we have here used a specific material, the ma-N 2410 resist, the method can be adapted to any kind of resist, positive or negative. Hence, this technique is a step toward proliferation and democratization of metasurface research.

As demonstrated here, critical point drying enables fabrication of ma-N 2410 resist metasurfaces with efficiency above 50%. It should, in principle, be possible to reach even higher efficiencies if the nanoparticles were made taller (aspect ratio > 25); however, fabricating such tall nanofins is challenging. A polymer with a higher refractive index would allow one to reach a high efficiency with shorter nanofins, but unmodified polymers with an index higher than 1.75 are difficult to come by.[50] One approach could be to instead use a polymer nanocomposite in which high-index dielectric or metallic nanoinclusions are used to increase the average refractive index of the nanofins.[51,52] It is, of course, also possible to use resists with a lower refractive index, since the required 2π phase coverage can be reached irrespective of refractive index given that the nanofins are sufficiently tall.[10] In this sense, the method demonstrated here is truly general.

Lastly, the resist used here can also be exposed by UV-lithography. Advanced deep-UV-lithography systems routinely expose patterns significantly smaller than the patterns exposed by EBL here, and reports on macroscopic metasurfaces made by UV-lithography have indeed already appeared.[53−55] Considering this, one might envision a scheme where UV-lithography is used to build large-scale polymer-based metasurfaces, further decreasing the processing time and eventually facilitating flat optical components to become a substantial competitor to bulk optics.

METHODS

Simulations. Numerical simulations (FDTD) were performed using commercial software (Lumerical). Dielectric nanofins made of ma-N 2410 were placed on a glass substrate (refractive index n = 1.5) and illuminated by left circularly polarized light from the substrate side. Periodic boundary conditions were used in the in-plane direction and perfectly matched layers in the out-of-plane direction. A transmission monitor was placed 2 μm above the nanofin on the air side and the complex electric field was recorded. To obtain the electric field decomposed into the circularly polarized basis, the field at the transmission monitor is averaged to be treated as a plane wave propagating normal to the surface. For wavelengths larger than the unit-cell period, the variations over the monitor are small enough to be attributed to computer rounding errors (<1%). For wavelengths smaller than the unit-cell, this approximation introduces errors since some light propagates with different k-vectors due to diffractive effects, and the simulation results in these wavelength ranges are treated as an approximation. Nevertheless, some of the spectral features in this range are observed also in the experimental verification.

Fabrication. Metasurface substrates are first cleaned by sonication in acetone and isopropanol, then treated with oxygen plasma to remove organic contaminants and water vapor. A layer of Ti-Prime is spin-coated on the substrate to increase resist adhesion, followed by spin coating of the resist (ma-N 2410, Micro Resist Technology GmbH, Germany). A prebake step is performed thereafter. For transparent samples, the surface is

https://dx.doi.org/10.1021/acsphotonics.9b01809
ACS Photonics 2020, 7, 885−892

then coated with a conductive polymer, which serves as a sacrificial layer, and a 15 nm layer of Cr, which renders the surface reflective during the subsequent electron-beam lithography exposure (Raith EBPG5200). The patterns are exposed with a current of 20 nA to a dose of 400 $\mu C/cm^2$. After the exposure, the sample is placed in water to lift off the conductive polymer and chromium, and then placed in a developer (ma-D 525) to uncover the metasurface. The sample is rinsed in water and then dried in a N_2 flow or through critical point drying.

To perform critical point drying, a solvent that is soluble in both water and liquid CO_2 and, at the same time, does not dissolve the resist is required. In previous publications, hexane has been found as a suitable solvent.[39,40] However, water is not soluble in hexane and therefore surfactants are added to both water and hexane to promote micelle formation upon mixing of the two liquids. Span 20 is dissolved in hexane and Tween 20 is added to water, producing a mixture with a hydrophilic−lipophilic balance suitable to generate water-containing micelles in hexane. The following drying procedure is subsequently followed: (1) The sample is moved from rinse water containing Tween 20 to the hexane/Span 20 mixture and vigorously shaken to aid micelle formation. (2) The sample is transferred to a beaker of pure hexane to wash away the water-containing micelles and subsequently to pure hexane in the critical point dryer. (3) The hexane is iteratively replaced with liquid CO_2, and when the concentration of hexane is low, the temperature/pressure in the chamber is raised to above 31 °C/74 bar. Here, the CO_2 enters its gas phase via a supercritical phase and can then be purged from the chamber, leaving a dried metasurface sample.

Optical Measurements. The optical experiments for this work were performed with a custom-built microscope setup. Polarization control of the light was obtained by using two sets of linear polarizers (LPVISE100-A) and achromatic quarter waveplates (AHWP05M-600). The white light illumination source used was a laser driven light source (Energetiq EQ-99XFC LDLS) that, if desired, can be spectrally filtered with a liquid crystal tunable filter (Varispec 420−730 nm). Moreover, three different lasers with blue, green, and red output lights were fiber-coupled to the system, namely, 447, 532, and 660 nm. The microscope objectives used for light collection and imaging were a 20×/0.75 (Nikon Plan Apo) or a 40×/0.95 (Nikon CFI Plan Apo Lambda), depending on the desired field of view and magnification. Images were collected with a CCD camera (Thorlabs DCC1545M), whereas spectra were recorded using a fiber-coupled spectrometer (Ocean Optics QE65000). Lastly, when detailed motion control was desired, optical components were mounted on a motorized one-axis translation stage (Thorlabs PT1-Z8).

■ ASSOCIATED CONTENT

Supporting Information

The Supporting Information is available free of charge at https://pubs.acs.org/doi/10.1021/acsphotonics.9b01809.

Optical parameters for the ma-N 2410 resist; Simulated polarization conversion efficiency versus fin height; Exemplary SEM images; Experimental setups for optical measurements; Simulation details for resist metasurfaces; Experimental polarized transmission curves; Simulated electric near-field intensity distribution for meta-atom; Results from imaging with a metalens; Results from a reflective metasurface; Optical inspection of the reflective metasurfaces (PDF)

■ AUTHOR INFORMATION

Corresponding Authors

Daniel Andrén − *Department of Physics, Chalmers University of Technology, S-412 96 Göteborg, Sweden;* orcid.org/0000-0003-0682-5129; Email: daniel.andren@chalmers.se

Mikael Käll − *Department of Physics, Chalmers University of Technology, S-412 96 Göteborg, Sweden;* orcid.org/0000-0002-1163-0345; Email: mikael.kall@chalmers.se

Ruggero Verre − *Department of Physics, Chalmers University of Technology, S-412 96 Göteborg, Sweden;* orcid.org/0000-0001-8337-9009; Email: ruggero.verre@chalmers.se

Authors

Jade Martínez-Llinàs − *Department of Physics, Chalmers University of Technology, S-412 96 Göteborg, Sweden;* orcid.org/0000-0003-3837-2582

Philippe Tassin − *Department of Physics, Chalmers University of Technology, S-412 96 Göteborg, Sweden*

Complete contact information is available at: https://pubs.acs.org/10.1021/acsphotonics.9b01809

Notes

The authors declare no competing financial interest.

■ ACKNOWLEDGMENTS

This work was supported by the Knut and Alice Wallenberg Foundation, the Swedish Foundation for Strategic Research, and the Excellence Initiative Nano at Chalmers University of Technology. This work was performed in part at Myfab Chalmers, and we would like to especially acknowledge the help from N. Lindvall and M. Rommel.

■ REFERENCES

(1) Luo, X. Subwavelength Artificial Structures: Opening a New Era for Engineering Optics. *Adv. Mater.* **2019**, *31* (4), 1804680.

(2) Yu, N.; Genevet, P.; Kats, M. A.; Aieta, F.; Tetienne, J.-P.; Capasso, F.; Gaburro, Z. Light Propagation with Phase Discontinuities: Generalized Laws of Reflection and Refraction. *Science (Washington, DC, U. S.)* **2011**, *334* (6054), 333−337.

(3) Aieta, F.; Genevet, P.; Kats, M. A.; Yu, N.; Blanchard, R.; Gaburro, Z.; Capasso, F. Aberration-Free Ultrathin Flat Lenses and Axicons at Telecom Wavelengths Based on Plasmonic Metasurfaces. *Nano Lett.* **2012**, *12* (9), 4932−4936.

(4) Lin, D.; Fan, P.; Hasman, E.; Brongersma, M. L. Dielectric Gradient Metasurface Optical Elements. *Science (Washington, DC, U. S.)* **2014**, *345* (6194), 298−302.

(5) Paniagua-Dominguez, R.; Yu, Y. F.; Khaidarov, E.; Choi, S.; Leong, V.; Bakker, R. M.; Liang, X.; Fu, Y. H.; Valuckas, V.; Krivitsky, L. A.; Kuznetsov, A. I. A Metalens with a Near-Unity Numerical Aperture. *Nano Lett.* **2018**, *18* (3), 2124−2132.

(6) Khorasaninejad, M.; Chen, W. T.; Devlin, R. C.; Oh, J.; Zhu, A. Y.; Capasso, F. Metalenses at Visible Wavelengths: Diffraction-Limited Focusing and Subwavelength Resolution Imaging. *Science (Washington, DC, U. S.)* **2016**, *352* (6290), 1190−1194.

(7) Wang, S.; Wu, P. C.; Su, V.-C.; Lai, Y.-C.; Chen, M.-K.; Kuo, H. Y.; Chen, B. H.; Chen, Y. H.; Huang, T.-T.; Wang, J.-H.; et al. A Broadband Achromatic Metalens in the Visible. *Nat. Nanotechnol.* **2018**, *13* (3), 227.

(8) Liang, H.; Lin, Q.; Xie, X.; Sun, Q.; Wang, Y.; Zhou, L.; Liu, L.; Yu, X.; Zhou, J.; Krauss, T. F; Li, J. Ultrahigh Numerical Aperture Metalens at Visible Wavelengths. *Nano Lett.* **2018**, *18* (7), 4460−4466.

(9) Chen, W. T.; Zhu, A. Y.; Khorasaninejad, M.; Shi, Z.; Sanjeev, V.; Capasso, F. Immersion Meta-Lenses at Visible Wavelengths for Nanoscale Imaging. *Nano Lett.* **2017**, *17* (5), 3188−3194.
(10) Khorasaninejad, M.; Capasso, F. Metalenses: Versatile Multifunctional Photonic Components. *Science (Washington, DC, U. S.)* **2017**, *358* (6367), No. eaam8100.
(11) Zhan, A.; Colburn, S.; Trivedi, R.; Fryett, T. K.; Dodson, C. M.; Majumdar, A. Low-Contrast Dielectric Metasurface Optics. *ACS Photonics* **2016**, *3* (2), 209−214.
(12) Ni, X.; Kildishev, A. V.; Shalaev, V. M. Metasurface Holograms for Visible Light. *Nat. Commun.* **2013**, *4*, 2807.
(13) Zheng, G.; Mühlenbernd, H.; Kenney, M.; Li, G.; Zentgraf, T.; Zhang, S. Metasurface Holograms Reaching 80% Efficiency. *Nat. Nanotechnol.* **2015**, *10* (4), 308.
(14) Wang, B.; Dong, F.; Li, Q.-T.; Yang, D.; Sun, C.; Chen, J.; Song, Z.; Xu, L.; Chu, W.; Xiao, Y.-F.; Gong, Q.; Li, Y. Visible-Frequency Dielectric Metasurfaces for Multiwavelength Achromatic and Highly Dispersive Holograms. *Nano Lett.* **2016**, *16* (8), 5235−5240.
(15) Khorasaninejad, M.; Crozier, K. B. Silicon Nanofin Grating as a Miniature Chirality-Distinguishing Beam-Splitter. *Nat. Commun.* **2014**, *5*, 5386.
(16) Mueller, J. P. B.; Rubin, N. A.; Devlin, R. C.; Groever, B.; Capasso, F. Metasurface Polarization Optics: Independent Phase Control of Arbitrary Orthogonal States of Polarization. *Phys. Rev. Lett.* **2017**, *118* (11), 113901.
(17) Martínez-Llinàs, J.; Henry, C.; Andrén, D.; Verre, R.; Käll, M.; Tassin, P. A Gaussian Reflective Metasurface for Advanced Wavefront Manipulation. *Opt. Express* **2019**, *27* (15), 21069−21082.
(18) Arbabi, A.; Arbabi, E.; Horie, Y.; Kamali, S. M.; Faraon, A. Planar Metasurface Retroreflector. *Nat. Photonics* **2017**, *11* (7), 415.
(19) Markovich, H.; Shishkin, I. I.; Hendler, N.; Ginzburg, P. Optical Manipulation along an Optical Axis with a Polarization Sensitive Meta-Lens. *Nano Lett.* **2018**, *18* (8), 5024−5029.
(20) Tkachenko, G.; Stellinga, D.; Ruskuc, A.; Chen, M.; Dholakia, K.; Krauss, T. F. Optical Trapping with Planar Silicon Metalenses. *Opt. Lett.* **2018**, *43* (14), 3224−3227.
(21) Arbabi, A.; Arbabi, E.; Kamali, S. M.; Horie, Y.; Han, S.; Faraon, A. Miniature Optical Planar Camera Based on a Wide-Angle Metasurface Doublet Corrected for Monochromatic Aberrations. *Nat. Commun.* **2016**, *7*, 13682.
(22) Lin, J. R.; Su, V.-C.; Wang, S.; Chung, T. L.; Chen, J.-W.; Wu, P. C.; Tsai, D. P.; Chen, J.; Li, T.; Zhu, S.; et al. Achromatic Metalens Array for Full-Colour Light-Field Imaging. *Nat. Nanotechnol.* **2019**, *14* (3), 227.
(23) Chen, B. H.; Wu, P. C.; Su, V.-C.; Lai, Y.-C.; Chu, C. H.; Lee, I C.; Chen, J.-W.; Chen, Y. H.; Lan, Y.-C.; Kuan, C.-H.; Tsai, D. P. GaN Metalens for Pixel-Level Full-Color Routing at Visible Light. *Nano Lett.* **2017**, *17* (10), 6345−6352.
(24) Faraji-Dana, M.; Arbabi, E.; Arbabi, A.; Kamali, S. M.; Kwon, H.; Faraon, A. Compact Folded Metasurface Spectrometer. *Nat. Commun.* **2018**, *9* (1), 4196.
(25) Ee, H.-S.; Agarwal, R. Tunable Metasurface and Flat Optical Zoom Lens on a Stretchable Substrate. *Nano Lett.* **2016**, *16* (4), 2818−2823.
(26) Afridi, A.; Canet-Ferrer, J.; Philippet, L.; Osmond, J.; Berto, P.; Quidant, R. Electrically Driven Varifocal Silicon Metalens. *ACS Photonics* **2018**, *5* (11), 4497−4503.
(27) Colburn, S.; Zhan, A.; Majumdar, A. Varifocal Zoom Imaging with Large Area Focal Length Adjustable Metalenses. *Optica* **2018**, *5* (7), 825−831.
(28) Rogers, E. T. F.; Lindberg, J.; Roy, T.; Savo, S.; Chad, J. E.; Dennis, M. R.; Zheludev, N. I. A Super-Oscillatory Lens Optical Microscope for Subwavelength Imaging. *Nat. Mater.* **2012**, *11* (5), 432.
(29) Li, Z.; Zhang, T.; Wang, Y.; Kong, W.; Zhang, J.; Huang, Y.; Wang, C.; Li, X.; Pu, M.; Luo, X. Achromatic Broadband Super-resolution Imaging by Super-oscillatory Metasurface. *Laser Photon. Rev.* **2018**, *12* (10), 1800064.
(30) Cohen, A. L. Multifocal Optical Device with Spurious Order Suppression and Method for Manufacture of Same. U.S. Patent US5120120A, June 9, 1992.
(31) Rahlves, M.; Rezem, M.; Boroz, K.; Schlangen, S.; Reithmeier, E.; Roth, B. Flexible, Fast, and Low-Cost Production Process for Polymer Based Diffractive Optics. *Opt. Express* **2015**, *23* (3), 3614−3622.
(32) Lim, K. T. P.; Liu, H.; Liu, Y.; Yang, J. K. W. Holographic Colour Prints for Enhanced Optical Security by Combined Phase and Amplitude Control. *Nat. Commun.* **2019**, *10* (1), 1−8.
(33) Pancharatnam, S. Generalized Theory of Interference and Its Applications. *Proc. - Indian Acad. Sci., Sect. A* **1956**, *44*, 398−417.
(34) Berry, M. V. The Adiabatic Phase and Pancharatnam's Phase for Polarized Light. *J. Mod. Opt.* **1987**, *34* (11), 1401−1407.
(35) Bomzon, Z.; Kleiner, V.; Hasman, E. Pancharatnam-Berry Phase in Space-Variant Polarization-State Manipulations with Subwavelength Gratings. *Opt. Lett.* **2001**, *26* (18), 1424−1426.
(36) Bomzon, Z.; Biener, G.; Kleiner, V.; Hasman, E. Space-Variant Pancharatnam-Berry Phase Optical Elements with Computer-Generated Subwavelength Gratings. *Opt. Lett.* **2002**, *27* (13), 1141−1143.
(37) Hasman, E.; Kleiner, V.; Biener, G.; Niv, A. Polarization Dependent Focusing Lens by Use of Quantized Pancharatnam-Berry Phase Diffractive Optics. *Appl. Phys. Lett.* **2003**, *82* (3), 328−330.
(38) Tanaka, T.; Morigami, M.; Atoda, N. Mechanism of Resist Pattern Collapse during Development Process. *Jpn. J. Appl. Phys.* **1993**, *32* (12S), 6059.
(39) Namatsu, H. Supercritical Drying for Water-Rinsed Resist Systems. *J. Vac. Sci. Technol., B: Microelectron. Process. Phenom.* **2000**, *18* (6), 3308−3312.
(40) Goldfarb, D. L.; de Pablo, J. J.; Nealey, P. F.; Simons, J. P.; Moreau, W. M.; Angelopoulos, M. Aqueous-Based Photoresist Drying Using Supercritical Carbon Dioxide to Prevent Pattern Collapse. *J. Vac. Sci. Technol., B: Microelectron. Process. Phenom.* **2000**, *18* (6), 3313−3317.
(41) Khorasaninejad, M.; Zhu, A. Y.; Roques-Carmes, C.; Chen, W. T.; Oh, J.; Mishra, I.; Devlin, R. C.; Capasso, F. Polarization-Insensitive Metalenses at Visible Wavelengths. *Nano Lett.* **2016**, *16* (11), 7229−7234.
(42) Shrestha, S.; Overvig, A. C.; Lu, M.; Stein, A.; Yu, N. Broadband Achromatic Dielectric Metalenses. *Light: Sci. Appl.* **2018**, *7* (1), 1−11.
(43) Kim, I.; Yoon, G.; Jang, J.; Genevet, P.; Nam, K. T.; Rho, J. Outfitting next Generation Displays with Optical Metasurfaces. *ACS Photonics* **2018**, *5* (10), 3876−3895.
(44) Burch, J.; Wen, D.; Chen, X.; Di Falco, A. Conformable Holographic Metasurfaces. *Sci. Rep.* **2017**, *7* (1), 4520.
(45) Fan, Q.; Huo, P.; Wang, D.; Liang, Y.; Yan, F.; Xu, T. Visible Light Focusing Flat Lenses Based on Hybrid Dielectric-Metal Metasurface Reflector-Arrays. *Sci. Rep.* **2017**, *7*, 45044.
(46) She, A.; Zhang, S.; Shian, S.; Clarke, D. R.; Capasso, F. Large Area Metalenses: Design, Characterization, and Mass Manufacturing. *Opt. Express* **2018**, *26* (2), 1573−1585.
(47) Lin, Z.; Liu, V.; Pestourie, R.; Johnson, S. G. Topology Optimization of Freeform Large-Area Metasurfaces. *Opt. Express* **2019**, *27* (11), 15765−15775.
(48) Khorasaninejad, M.; Aieta, F.; Kanhaiya, P.; Kats, M. A.; Genevet, P.; Rousso, D.; Capasso, F. Achromatic Metasurface Lens at Telecommunication Wavelengths. *Nano Lett.* **2015**, *15* (8), 5358−5362.
(49) Sawant, R.; Bhumkar, P.; Zhu, A. Y.; Ni, P.; Capasso, F.; Genevet, P. Mitigating Chromatic Dispersion with Hybrid Optical Metasurfaces. *Adv. Mater.* **2019**, *31* (3), 1805555.
(50) Liu, J.; Ueda, M. High Refractive Index Polymers: Fundamental Research and Practical Applications. *J. Mater. Chem.* **2009**, *19* (47), 8907−8919.
(51) Pradana, A.; Kluge, C.; Gerken, M. Tailoring the Refractive Index of Nanoimprint Resist by Blending with TiO 2 Nanoparticles. *Opt. Mater. Express* **2014**, *4* (2), 329−337.
(52) Hemmati, H.; Magnusson, R. Development of Tuned Refractive-Index Nanocomposites to Fabricate Nanoimprinted Optical Devices. *Opt. Mater. Express* **2018**, *8* (1), 175−183.

https://dx.doi.org/10.1021/acsphotonics.9b01809
ACS Photonics 2020, 7, 885−892

(53) Li, N.; Fu, Y. H.; Dong, Y.; Hu, T.; Xu, Z.; Zhong, Q.; Li, D.; Lai, K. H.; Zhu, S.; Lin, Q.; Gu, Y.; Singh, N. Large-Area Pixelated Metasurface Beam Deflector on a 12-Inch Glass Wafer for Random Point Generation. *Nanophotonics* **2019**, *8* (10), 1855−1861.
(54) Xu, Z.; Dong, Y.; Tseng, C.-K.; Hu, T.; Tong, J.; Zhong, Q.; Li, N.; Sim, L.; Lai, K. H.; Lin, Y.; et al. CMOS-Compatible All-Si Metasurface Polarizing Bandpass Filters on 12-Inch Wafers. *Opt. Express* **2019**, *27* (18), 26060−26069.
(55) Park, J.-S.; Zhang, S.; She, A.; Chen, W. T.; Lin, P.; Yousef, K. M. A.; Cheng, J.-X.; Capasso, F. All-Glass, Large Metalens at Visible Wavelength Using Deep-Ultraviolet Projection Lithography. *Nano Lett.* **2019**, *19*, 8673−8682.

https://dx.doi.org/10.1021/acsphotonics.9b01809
ACS Photonics 2020, 7, 885−892